JOURNAL OF SOLID STATE CHEMISTRY 104, 239–252 (1993)

Sn–K and Pb–L_3 EXAFS, X-Ray Diffraction, and ^{119}Sn Mössbauer Spectroscopic Studies of Ordered β-$PbSnF_4$ and Disordered $Pb_{1-x}Sn_xF_2$ (x = 0.3, 0.4) Solid Solutions and $PbSn_4F_{10}$: High Performance Fluoride Ion Conductors

G. DENES*

Laboratory of Solid State Chemistry and Mössbauer Spectroscopy, Department of Chemistry and Laboratories for Inorganic Materials, Concordia University, 1455 De Maisonneuve Blvd. W., Montreal, Quebec, Canada H3G 1M8

AND Y. H. YU, T. TYLISZCZAK, AND A. P. HITCHCOCK

Institute for Materials Research, McMaster University, Hamilton, Ontario, Canada L8S 4M1

Received August 14, 1991; in revised form October 7, 1992; accepted October 9, 1992

Fully and partly disordered superionic conductors in the PbF_2/SnF_2 system have been studied using X-ray powder diffraction, ^{119}Sn Mössbauer spectroscopy, and Pb–L_3 and Sn–K EXAFS (extended X-ray absorption fine structure). X-ray diffraction is seriously limited because of the large degree of disorder at the metal site. The solid solution $Pb_{1-x}Sn_xF_2$ (x = 0–0.30) is fully disordered as is the stoichiometric compound $PbSn_4F_{10}$ (x = 0.80). On the other hand, some degree of ordering occurs in $Pb_{0.6}Sn_{0.4}F_2$ (x = 0.40) and β-$PbSnF_4$ (x = 0.50). ^{119}Sn Mössbauer spectra show that the tin(II) lone pair is stereoactive in these materials. Therefore, the tin environment is highly distorted and its nonbonded electron pair is not a charge carrier in the conduction mechanism. The Sn–K and Pb–L_3 EXAFS spectra indicate average first shell distances of R_{Sn-F} = 2.12(1) Å and R_{Pb-F} = 2.55(1) Å. There is a clear second shell Pb–Pb signal in the Pb–L_3 EXAFS but no higher shell signal in the Sn–K EXAFS, indicating a higher degree of disorder and a lower rigidity of next-neighbor fluorine shells around Sn than around Pb. The results are discussed in relation to previous studies of ordered $MSnF_4$ fluoride ionic conductors and to proposed mechanisms for ionic conduction in these superionic materials.

I. Introduction

Superionic conductors are solid materials that have ionic conductivity similar to that of ionic liquids. The conductivity mechanism in ionic conductor varies with the crystal structure of the material. Examples include (i) long range partially occupied planes (β-aluminas) or tunnels (NASICON), (ii) ion disorder over several sites with partial occupancy factors (α-AgI and $RbAg_4I_5$), and (iii) point defects (Frenkel defects for fluorite type structures, and Schottky defects in many close packed ionic structures) (*1*). The ionic conductivity of β-PbF_2 and BaF_2 can be boosted by about three orders of magnitude by replacement of half of the Pb (Ba) by Sn(II) (*2, 3*). The resulting α-$PbSnF_4$ and $BaSnF_4$ compounds show a tetragonal distortion of the cubic fluorite type; they have a strongly anisotropic structure, with Pb (Ba) and Sn being ordered (*4–6*).

* To whom all correspondence should be addressed.

0022-4596/93 $5.00

Other related phases can be prepared in the PbF_2/SnF_2 pseudobinary system, which have superionic properties approaching those of $PbSnF_4$, the latter being the best known fluoride ion conductor. In earlier work, one of us prepared a wide range of $Pb_{1-x}Sn_xF_2$ (x = 0–0.50) solid solutions (*7*). These can be divided into two structural regimes: (i) for x = 0 to 0.30, the symmetry is cubic, space group $Fm3m$, identical to the fluorite type β-PbF_2; and (ii) for x = 0.30 to 0.50, there is a tetragonal distortion of the fluorite type with a very large supercell (cell volume multiplied by 32). The fluoride ion mobility in these solid solutions has been studied with the help of conductivity measurements and ^{19}F nuclear magnetic relaxation (*7, 8*). In addition, Denes and co-workers have prepared β-$PbSnF_4$ (*5*) and $PbSn_4F_{10}$ (*9*), two high temperature phases which are quenchable to room temperature in a metastable state. The absence of Pb/Sn long range order in $PbSn_4F_{10}$ and in the $Pb_{1-x}Sn_xF_2$ (x = 0 to 0.30) cubic solid solution, as witnessed by the surprising simplicity of their X-ray powder pattern (no symmetry break and no superstructure), precludes a detailed structural study by diffraction techniques. The large superstructure of β-$PbSnF_4$ and of the partially disordered tetragonal solid solution seriously reduces the effectiveness of diffraction studies. Another limiting factor is that only powder diffraction studies are possible since single crystals of these materials have not yet been prepared.

In this paper, we present a study of $Pb_{1-x}Sn_xF_2$ as a cubic solid solution (x = 0.30) and a tetragonal solid solution (x = 0.40), β-$PbSnF_4$ (x = 0.5), and $PbSn_4F_{10}$ (x = 0.8). X-ray powder diffraction shows that there is no long range order in $PbSn_4F_{10}$ and the cubic solid solution, and indicates that there is a considerable local disorder. X-ray diffraction of β-$PbSnF_4$ and the tetragonal solid solution (x = 0.40) shows tetragonal distortion, the presence of a large superstructure, and that there is a partial disorder between Pb and Sn in the tetragonal solid solution. ^{119}Sn Mössbauer spectroscopy shows that, in all the compounds studied, the tin coordination is very strongly distorted, with the tin(II) lone pair being stereoactive. Therefore, substitution of Pb by Sn must result in a very large local rearrangement of the lattice. In addition, since the lone pair of each tin atom is localized it cannot be a charge carrier in the conduction mechanism.

EXAFS (Extended X-ray Absorption Fine Structure) is very useful for studying the local environment of particular atoms, regardless of the degree of crystallinity of the material, and it has been successfully applied to studies of superionic conductors (*10–13*). EXAFS studies below and above the superionic transition of several cationic conductors have yielded invaluable information about the correlations between the mobile ions and the fixed sublattice of the counterions (*12*). Recently we have reported a combined EXAFS, X-ray diffraction, and Mössbauer study of ordered $MSnF_4$ (M = Pb and Ba) fluoride ionic conductors (*13*). In the work presented here, the same three techniques are used to investigate the structure of materials with the composition $Pb_{1-x}Sn_xF_2$ (x = 0.3, 0.4, 0.5, and 0.8), where the disorder is much larger than in those samples studied earlier (*13*).

II. Experiments, Materials, and Data Analysis

PbF_2 (99.9%, Alfa); SnF_2 (99.8%, Sharpe Chemical), and SnO (Omnium Scientific) were used in the syntheses and/or as EXAFS standards. All the $Pb_{1-x}Sn_xF_2$ materials were prepared according to the following procedure: appropriate stoichiometric mixtures of SnF_2 and PbF_2 were thoroughly mixed and ground together in an agate mortar, then loaded into a copper tube previously sealed at one end and put in the port of a dry nitrogen globe box. After evacuating the port, flushing it with nitrogen, and temporarily sealing the tube inside the glove box, final sealing of the second end was per-

TABLE I

THICKNESS OF SAMPLES USED FOR MÖSSBAUER ABSORPTION SPECTROSCOPY

x	Formula	m (mg)	wt% Sn	mg Sn/cm^2
0.80	$PbSn_4F_{10}$	180	54	25.8
0.50	β-$PbSnF_4$	165	30	13.0
0.40	$Pb_{0.6}Sn_{0.4}F_2$	157	23	9.3
0.30	$Pb_{0.7}Sn_{0.3}F_2$	100	16	4.3

Note. x = tin stoichiometry in $Pb_{1-x}Sn_xF_2$; m (mg) = sample mass; wt% Sn = weight % Sn in the sample; mg Sn/cm^2 = weight of tin (natural isotopic abundance) in the sample, per unit surface (in mg).

formed outside the glove box, according to the procedure described in (*14*). In all cases, the copper tubes were preheated for 1 hr at 200°C, just below the melting point of SnF_2 (215°C). With this procedure SnF_2 reacts with PbF_2 in the solid state, thereby avoiding corrosion by liquid SnF_2. In a second step, the tubes were heated for a period of 1 to 4 hr at the temperature required to complete the reaction and obtain the phase of interest (500°C for the solid solutions and β-$PbSnF_4$, and 250°C for $PbSn_4F_{10}$). Then the tubes were quenched by quick immersion in cold water, in order to stabilize the high temperature metastable phases of interest. Quenching has to be very quick for β-$PbSnF_4$, and especially for $PbSn_4F_{10}$, which is the least stable of the compounds investigated (*9*). On the other hand, once quenched to room temperature, the solid solutions have shown no sign of decomposition after storage for several years at ambient temperature in plastic containers.

X-ray powder diffraction was carried out on a PW 1050-25 Philips diffractometer, using Ni-filtered Cu$K\alpha$ radiation (λ = 1.54178 Å). For ^{119}Sn Mössbauer spectroscopy, the γ-ray source was 15 mCi $Ca^{119m}SnO_3$ (Amersham) and the Doppler velocity was obtained using an Elscint drive system working in the constant acceleration mode. The amount of sample used was small, especially at low x values, because of the high amount of nonresonant absorption by lead (Table I). This resulted in very thin samples (in terms of amount of tin per unit surface), and therefore a low signal/background ratio. However, it was the best compromise between too thin a sample and too low a count rate. The samples were contained in a sealed Teflon sample holder at 25°C. The transmitted γ-rays were detected using a Harshaw (Tl)NaI scintillation detector and the spectra were accumulated in a multichannel analyzer operating in the multiscaling mode. Computer fitting was performed using the GMFP5 program (*15*), which is a modified version of the GMFP software of Ruebenbauer and Birchall (*16*).

X-ray absorption spectra at the Sn–K (29.3 keV) and Pb–L_3 (13.035 keV) edges were recorded in transmission mode using the C-2 beam line of the Cornell high energy synchrotron source (CHESS). Experimental details have been discussed elsewhere (*13, 17, 18*). As in previous work (*13*), the data processing was carried out with conventional Fourier filter and k-space curve-fit techniques (*19, 20*) using both calculated spherical wave amplitude and phase functions (*21*) and experimental standards (β-PbF_2 and SnO (*13*)) to derive distance, coordination number, and Debye–Waller ($\Delta\sigma^2$) information. k^1-weighting of the data was used in all analyses.

III. Results and Discussion

3.1. Unit-Cell

The unit-cell parameters of β-PbF_2 and the compounds under investigation, refined from the X-ray powder diffraction data using the program PAFI of Le Marouille (*22*), are given in Table II. $Pb_{0.70}Sn_{0.30}F_2$ and $PbSn_4F_{10}$ have a cubic $Fm3m$ unit-cell identical to that of β-PbF_2, with a very similar edge length. On the other hand, $Pb_{0.60}Sn_{0.40}F_2$ and β-$PbSnF_4$ have a very large tetragonal unit cell, with $a \approx 17$ Å, $c \approx 23$ Å, and $V \approx 6500$ Å^3 for both compounds. This large cell is a super-cell of that of β-PbF_2 with, in addition, a tetragonal distortion (Fig. 1). It is also a supercell of that of α-$PbSnF_4$, although with a smaller tetrag-

TABLE II

UNIT-CELL PARAMETERS OF β-PbF_2 ($x = 0$), $Pb_{1-x}Sn_xF_2$ ($x = 0.30$ AND 0.40), β-$PbSnF_4$ ($x = 0.50$), AND $PbSn_4F_{10}$ ($x = 0.80$)

x[a]	0	0.30	0.40	0.50	0.80
a (Å)	5.940	5.916(1)	16.822(5)	16.834(5)	5.9541(5)
c (Å)	—	—	23.110(9)	23.063(13)	—
V (Å^3)	209.6	207.1(1)	6540(6)	6535(8)	211.1(3)
c/a[b]	1	1	0.9714(4)	0.9687(9)	1
Z[c]	4	4	128	128	4
C. S.[d]	cubic	cubic	tetragonal	tetragonal	cubic
S. G.[e]	$Fm3m$	$Fm3m$	—	—	$Fm3m$

[a] x is the substitution rate of Pb by Sn in $Pb_{1-x}Sn_xF_2$.
[b] For $x = 0.40$ and 0.50, c/a is multiplied by $\sqrt{2}$ to account for the axes change, in order to compare to undistorted β-PbF_2.
[c] Z = Number of MF_2 units per unit cell.
[d] C. S. = Crystal system.
[e] S. G. = Space group.

onal distortion ($c/a = 0.9687$ for β-$PbSnF_4$ and 0.9564 for α-$PbSnF_4$). The cell parameters and volume of β-$PbSnF_4$ (a_β, b_β, c_β, V_β) are simply related to those of β-PbF_2 (a_F, b_F, c_F, V_F) and those of α-$PbSnF_4$ (a_α, b_α, c_α, V_α) as follows:

$$a_\beta = b_\beta = 2\sqrt{2}.\, a_F = 4a_\alpha \qquad \text{(I)}$$

$$c_\beta = 4a_F = 2c_\alpha \qquad \text{(II)}$$

$$V_\beta = a_\beta.b_\beta.c_\beta = 32V_F = 32V_\alpha. \qquad \text{(III)}$$

The above relationships were established from the X-ray powder diffraction patterns (Fig. 2) which show the following:

(i) The tetragonal distortion splits all (hkl) peaks with $l \neq h$ which are observed in β-PbF_2;

(ii) The 45° rotation of the axes in the (**a**, **b**) plane changes the h and k Miller indices of all peaks, except (00l). The **a** and **b** axes of β-$PbSnF_4$ have twice the length of the

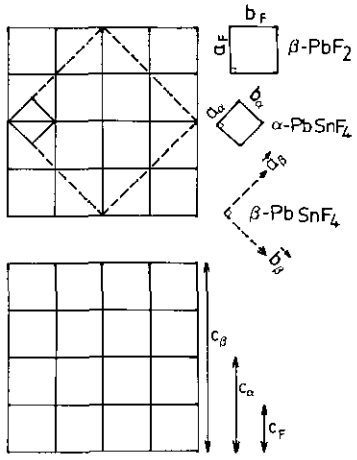

FIG. 1. Relationships between the unit cells of cubic β-PbF_2 fluorite type ($\mathbf{a}_F$, $\mathbf{b}_F$, $\mathbf{c}_F$), tetragonal α-$PbSnF_4$ ($\mathbf{a}_\alpha$, $\mathbf{b}_\alpha$, $\mathbf{c}_\alpha$), and tetragonal β-$PbSnF_4$ ($\mathbf{a}_\beta$, $\mathbf{b}_\beta$, $\mathbf{c}_\beta$).

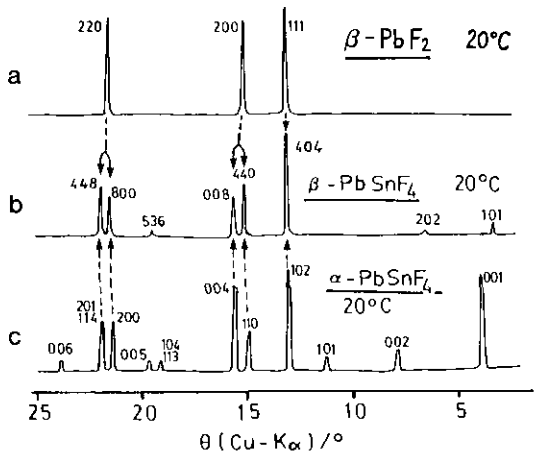

FIG. 2. Relationships between the X-ray powder pattern of (a) β-PbF_2 fluorite type, (b) β-$PbSnF_4$, and (c) α-$PbSnF_4$.

TABLE III

^{119}Sn MÖSSBAUER SPECTROSCOPIC RESULTS FOR $Pb_{1-x}Sn_xF_2$ (x = 0.30 AND 0.40), β-$PbSnF_4$ (x = 0.50), AND $PbSn_4F_{10}$ (x = 0.80)

Compound	δ (mm/s)[a]	Δ (mm/s)	Γ (mm/s)	Ref.
$PbSn_4F_{10}$	3.45(1)	1.45(1)	0.63(1)	(9)
$Pb_{0.70}Sn_{0.30}F_2$	3.07(2)	1.64(4)	0.76(7)	This work
$Pb_{0.60}Sn_{0.40}F_2$	3.25(2)	1.69(3)	0.72(5)	This work
β-$PbSnF_4$	3.06(2)	1.66(2)	0.68(3)	This work
α-$PbSnF_4$	3.25(1)	1.52(2)	0.66(4)	(6)
α-SnF_2	3.430(3)	1.532(3)	0.594(7)	(23)
$CsSnBr_3$	3.93	0	—	(27)

Note. Results for α-SnF_2, α-$PbSnF_4$, and $CsSnBr_3$ are given for comparison.
[a] Isomer shifts are referenced to $CaSnO_3$ as zero shift at room temperature.

diagonal of the (**a**, **b**) face of β-PbF_2, and four times the a and b parameters of α-$PbSnF_4$;

(iii) The length of the unit cell along the **c** axis is quadrupled in β-PbF_2, and doubled in α-$PbSnF_4$. This results in a quadrupling of the l index of β-PbF_2 and a doubling of the l index of α-$PbSnF_4$;

(iv) The large cell and reduction in symmetry from cubic to tetragonal makes new peaks appear. The superstructure reflections observed for β-$PbSnF_4$ are the same as those for $Pb_{0.60}Sn_{0.40}F_2$; however, they are not the same as for α-$PbSnF_4$.

The combination of the above four effects results in new peaks in β-$PbSnF_4$ [$(101)_\beta$, $(202)_\beta$, $(536)_\beta$] and a change of $(hkl)_F$ indexation of β-PbF_2 and of $(hkl)_\alpha$ indexation of α-$PbSnF_4$ peaks to give $(hkl)_\beta$ for β-$PbSnF_4$ according to

$$(111)_F \rightarrow (404)_\beta \leftarrow (102)_\alpha$$

$$(200)_F \rightarrow (440)_\beta \text{ and } (008)_\beta \leftarrow (110)_\alpha \text{ and } (004)_\alpha$$

$$(220)_F \rightarrow (800)_\beta \text{ and } (448)_\beta \leftarrow (200)_\alpha \text{ and } (114)_\alpha.$$

3.2 Interatomic Distances and Coordination.

The analogy between the unit-cells of β-PbF_2, and α- and β-$PbSnF_4$ suggests that their structures must be closely related. Since the unit-cells of $Pb_{0.70}Sn_{0.30}F_2$ and $PbSn_4F_{10}$ are identical to that of β-PbF_2 with no change of space group and no superstructure or distortion, one must conclude that the two metals are completely disordered. Since the unique cationic site in the fluorite structure has cubic coordination, one could believe that tin has no choice but to randomly substitute for lead in the center of the F_8 cubes. Fortunately, ^{119}Sn Mössbauer spectroscopy (Fig. 3) provides a convenient method for probing the local environment of tin, regardless of lattice symmetry or atomic order. The Mössbauer parameters given in Table III show that the isomer shift and quadrupole splitting for $Pb_{0.7}Sn_{0.3}F_2$ and $PbSn_4F_{10}$ are similar to the values observed

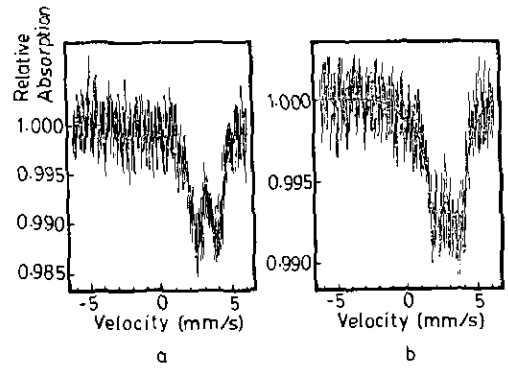

FIG. 3. ^{119}Sn Mössbauer spectrum of (a) β-$PbSnF_4$ and (b) $Pb_{0.7}Sn_{0.3}F_2$ at 298 K.

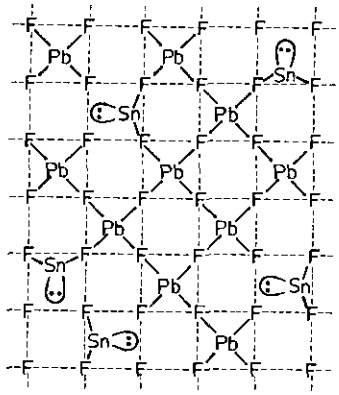

FIG. 4. Random substitution of Pb by Sn in the β-PbF_2 lattice, with random orientation of the tin(II) lone pair axis along the three crystallographic axes.

in α-SnF_2 (*23*) and α-$PbSnF_4$ (*6*). Of particular importance is the large value of the quadrupole splitting (Fig. 3), which shows that the tin(II) hybridization is $5s^{2-x}5p^x$ with possibly some $5d$ orbital contribution. Therefore the tin nonbonded electron pair has considerable p_z character and is stereoactive. The tin coordination is highly distorted in a direction opposite to the general direction of Sn–F bonding because of the large volume the lone pair occupies on the surface of the atom (*24–26*). This contrasts with compounds like $CsSnBr_3$ (*27*) which have a nonhybridized $5s^25p^0$ lone pair. In such species the nondirectional $5s$ orbital results in a high symmetry environment ($CsSnBr_3$ is cubic, perovskite type, with regular octahedral coordination about the Sn(II) atom). The hybridization of the $5s$ and $5p$ orbitals of tin in our materials is further corroborated by the high value of the isomer shift, characteristic of the divalent state (large s electron density at tin); however, the isomer shift is significantly lower than in $CsSnBr_3$ because some of the $5s$ electron density is used for bonding and is therefore shifted away from the tin atom.

The combination of X-ray powder diffraction and Mössbauer spectroscopy shows that Sn and Pb are disordered in the F_8 fluoride cubes, and that Sn is not in a regular cubic environment. Since lattice distortion is not observed, the primitive cubic sublattice of fluorine is preserved. It is likely that Sn(II) and its lone pair randomly substitute for Pb. Since a tin(II) lone pair occupies a volume similar to a fluoride ion (*25*), the most probable situation is that the lone pair goes in the middle of the F_8 cube and the tin atom is shifted, most likely toward a face of the cube, to give a square pyramidal coordination (Figs. 4 and 5b), similar to that observed in SnO (*28*). Such a situation, which has already been described in detail for $PbSn_4F_{10}$ (*9*), results in four equal Sn–F bonding distances of approximately 2.15–2.20 Å. The lead coordination should remain unchanged in this structural model, with eight equal Pb–F distances of 2.55–2.60 Å. Some local distortion at the lead atoms sharing fuorines with tin is possible, since one expects the fluorine atoms to be unequally shared, with more covalency in bonding to tin. It is not too surprising that β-PbF_2 can accommodate a small amount of tin(II) without long range lattice distortion (see Fig. 4). However, the wide range of cubic solution (substitution of up to 30% Pb) is quite surprising. Even more astounding is the compound $PbSn_4F_{10}$, where 80% of Pb is replaced by Sn, and the cubic symmetry of the lattice is conserved, with no superstructure. The fact that $PbSn_4F_{10}$ has a very specific stoichiometry (i.e., there is no detectable solid solution at

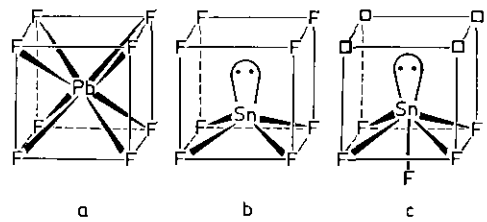

FIG. 5. Coordination of Pb and Sn in the lead(II) tin(II) fluorides: (a) cubic PbF_8 coordination, (b) square pyramidal SnF_4E coordination in β-$PbSnF_4$, $PbSn_4F_{10}$, and the cubic and tetragonal solid solutions, and (c) pseudo-octahedral SnF_5E coordination in α-$PbSnF_4$ (□ is a F vacancy).

adjacent compositions) is also very strange. This problem has been discussed in detail in an earlier study by Denes (*9*), who attributed the low stability of the $PbSn_4F_{10}$ structure at 25°C to its unusual—apparently illogical—structure. On the other hand, the cubic solid solution ($x = 0$–0.30) seems to be indefinitely stable at ambient temperature. This can be attributed to the lower rate of substitution, which is within the limits of strain which the β-PbF_2 structure can accommodate without distorting.

On the other hand, the tetragonal solid solution ($x = 0.31$–0.50), with β-$PbSnF_4$ as one of its limiting compositions, can no longer take additional tin without lattice distortion. In addition, the presence of superstructure reflections in the X-ray powder pattern shows that there is some order of tin and lead. However, it is more complicated than in α-$PbSnF_4$, since it involves a larger cell (c is quadrupled) and is not restricted to the **c** direction. With only three superstructure Bragg peaks available it is impossible to understand metal ordering in these phases. Since β-$PbSnF_4$ is at the limit of solubility of Sn in the solid solution, one can hypothesize that β-$PbSnF_4$ is completely ordered, with a minimum of two metal sites, A (100% Pb) and B (100% Sn). The tetragonal solid solution also shows the same type of ordering as β-$PbSnF_4$. However, since its composition is variable ($0.3 < x < 0.5$), the B site has a composition that varies from 60% Sn ($x = 0.30$) to 100% Sn ($x = 0.5$, β-$PbSnF_4$). Since the solid solution does not extend above $x = 0.50$, the A site remains entirely populated by Pb and cannot be substituted by Sn. This is probably necessary in order to keep the network of F_8 quasi-cubes stable. $PbSn_4F_{10}$ is an exception to this rule for reasons that are not understood.

In the tetragonal solid solution and β-$PbSnF_4$ one can assume that the coordination of lead is very similar to the cubic coordination found in β-PbF_2. The tin coordination is most likely 4 (square pyramidal) as in the cubic solid solution and in $PbSn_4F_{10}$, instead of 5 as in α-$PbSnF_4$. This is derived from the phase transitions observed in $PbSnF_4$ (*5*, *6*). Since the $\beta \rightarrow \gamma$ transition of $PbSnF_4$ is sharp and reversible with little hysteresis (the γ-phase, cubic space group $Fm3m$ identical to β-PbF_2, is not quenchable) it most likely involves small atomic shifts (displacive transition) rather than major structural rearrangements. On the other hand, the $\alpha \rightarrow \beta$ transition is sluggish and poorly reversible (the β-phase is easily quenchable). Therefore it involves bond breaking and atomic diffusion over considerable distances (reconstructive transition). The $\alpha \rightarrow \beta$ transition most likely involves a change of coordination of tin from 5 to 4, whereas in the $\beta \rightarrow \gamma$ transition, the tin coordination remains 4. The tetragonal distortion of β-$PbSnF_4$ is smaller than that of α-$PbSnF_4$ (c/a is closer to 1 for the β-phase). This is consistent with fluorine atoms located between the tin layers being present as a fluorine plane in β-$PbSnF_4$, instead of inside F_8 cubes as in α-$PbSnF_4$ (Fig. 5). This probably also explains why the anisotropy in β-$PbSnF_4$ is not quite as large as in the α-phase, since this fluorine layer provides some binding interactions (weak secondary bonding) between the metal/fluorine layers.

3.3. EXAFS

The structural information obtained from X-ray powder diffraction and Mössbauer spectroscopy is corroborated and supplemented by the EXAFS results. The Fourier transform (FT) magnitudes of the k^1-weighted Sn–K EXAFS of $Pb_{0.7}Sn_{0.3}F_2$ and $PbSn_4F_{10}$ are presented in Fig. 6, while the Pb–L_3 EXAFS of $PbSn_4F_{10}$, β-$PbSnF_4$, $Pb_{0.6}Sn_{0.4}F_2$ and $Pb_{0.7}Sn_{0.3}F_2$ are presented in Fig. 7. The average M–F first shell distances and coordination numbers, derived using phase and amplitude functions from spherical wave calculations (*21*) and experimental models, are presented in Table IV in comparison with diffraction results. β-PbF_2 and SnO have been used as experimental Pb–F and Sn–F standards, as in our previous work (*13*).

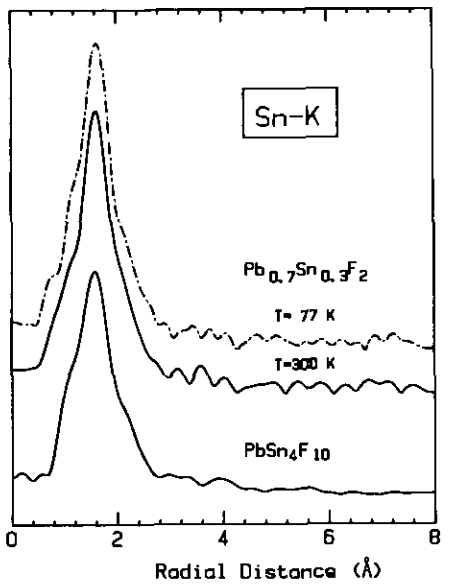

FIG. 6. Magnitude of the Fourier transforms of the k^1-weighted Sn–K EXAFS (2.5 to 12.5 Å^{-1}) of $Pb_{0.7}Sn_{0.3}F_2$ recorded at 300 and 77 K and of $PbSn_4F_{10}$ (300 K only). A common vertical scale is used.

The FT magnitudes of the Sn–K EXAFS (Fig. 6) exhibit a relatively broad, partially structured first-shell Sn–F signal with essentially no signal from more distant atoms, even in the 77 K data for $Pb_{0.7}Sn_{0.3}F_2$. The main effect of increased temperature (77 → 300 K) is to broaden the base of the main peak in the FT magnitude, although detailed analysis indicates that the Debye–Waller parameter does not change greatly with temperature (Table IV). This suggests that the fluoride ions adopt a wider range of positions at higher temperature (i.e., increased static disorder), consistent with the F atoms associated with the Sn site being involved in ionic conduction (*13*). The first shell peak in the FT of the Sn–K EXAFS exhibits both low- and high-R shoulders suggesting there are several closely spaced Sn–F distances which are not resolvable by EXAFS. We have explored multicomponent curve fits, based on the room temperature Sn–O first-shell EXAFS data as a model, to see if further quantitative information could be extracted. Good quality two-component fits were obtained and the two Sn–F distances derived (see Table V) are in reasonable agreement with those determined by diffraction for related species ($BaSnF_4$ (*13*)). However, the quality of a one-component fit is almost as good as that to two components, so we are hesitant to conclude that the two-component model explains the EXAFS results significantly better than a single average Sn–F distance. The average Sn–F distance (2.12 Å) derived using the experimental models is slightly shorter than that expected (2.15–2.20 Å (*9*)). This may be a result of the use of SnO as the source of the model phases. However, the difference is

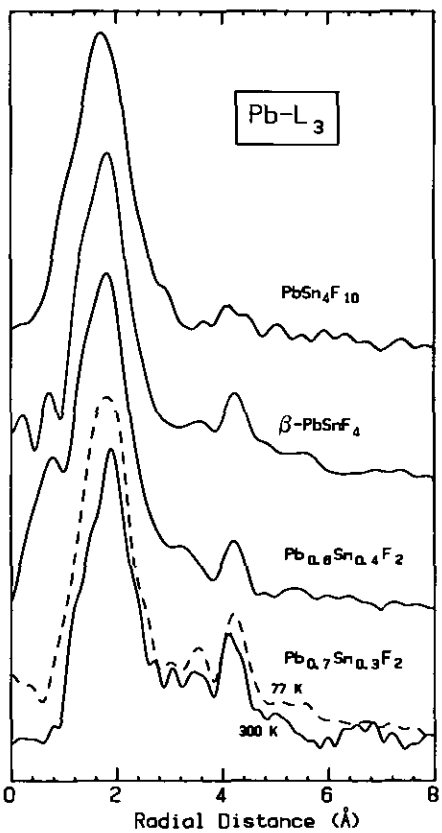

FIG. 7. Magnitude of the Fourier transforms of the Pb–L_3 EXAFS (2.6 to 12.0 Å^{-1}) of $PbSn_4F_{10}$, β-$PbSnF_4$, $Pb_{0.6}Sn_{0.4}F_2$ (recorded at 300 K), and $Pb_{0.7}Sn_{0.3}F_2$ (recorded at 77 and 300 K). A common vertical scale is used.

TABLE IV

INTERATOMIC DISTANCES AND COORDINATION NUMBERS DERIVED FROM EXAFS AND FROM X-RAY DIFFRACTION

	EXAFS[a]							
		calc.	expt.			Diffraction[b]		
Species	T(K)	R(Å)	R(Å)	N	$\sigma^2(10^{-3}$ Å$^2)$[c]	d(Å)	N	Ref.
⟨Sn–F distances (Sn–K)⟩								
$PbSn_4F_{10}$	300	2.15(3)	2.12	3.4	0.6	2.17	4	(9)
$Pb_{0.70}Sn_{0.30}F_2$	300	2.12	2.12	4.0	−0.5	2.17	4	TW
	77	2.14	2.12	4.4	−0.8	≈2.17	4	TW
SnO	300	2.22(1)	(2.22)	(4)	3.8[d]	2.22(2)	4	(25)
⟨Pb–F distances (Pb–L_3)⟩								
$PbSn_4F_{10}$	300	2.51(2)	2.52	6.8	6.2	2.578	8	(9)
β-$PbSnF_4$	300	2.51(2)	2.53	5.2	−2.2	2.57	8	TW
$Pb_{0.60}Sn_{0.40}F_2$	300	2.56(2)	2.55	5.7	−1.1	2.57	8	TW
$Pb_{0.70}Sn_{0.30}F_2$	300	2.59(2)	2.54	5.9	−1.7	2.57	8	TW
	77	2.56(2)	2.57	4.8	−7.1	≈2.57	8	TW
β-PbF_2	300	2.56(2)	(2.62)	(8)	13.4[d]	2.578	8	(1)

[a] EXAFS results (first shell average M–X distance; errors are statistical only and do not incorporate systematic errors such as those associated with phase transferability or accuracy of calculated phase functions. calc.: distances derived using spherical wave calculated phases (*21*). expt.: distances, coordination number, and Debye–Waller (DW) parameters derived using experimental phase and amplitude models from the first shell Sn–K EXAFS of SnO (300 K), Pb–L_3 EXAFS of β-PbF_2 (300 K), and N: coordination number (±20%). The ranges analyzed were 2.5–12.5 Å^{-1} in k-space and 0.8–3.0 Å for the Sn–K analysis, and 0.6–3.2 Å^{-1} (k) and 2.6–12.0 Å (R) for the Pb–L_3 analysis. The Fourier filter used no apodization on the forward transform while a symmetric Hanning window over 30% of the R-space range was used in the reverse transform.

[b] Diffraction results: $d(M–X)$: M–X distances in Å (M = Sn or Pb; X = F or O). N: coordination number. Ref.: reference number. TW: this work.

[c] This EXAFS DW parameter is the difference between the unknown and the model in the mean square displacement along the bond.

[d] DW derived using calculated amplitude functions (*21*); i.e., σ^2 (model) = 0.

not very significant, since the expected value is obtained from an idealized model of a system that is obviously disordered. In addition, we note that analysis with a spherical wave calculated phase function (*21*) predicts a Sn–F bond length longer by 0.02–0.03 Å. Therefore, considering the difficulty in obtaining structural information because of disorder, we can conclude that the EXAFS results are fully consistent with the information obtained by the other techniques.

In the Pb–L_3 EXAFS (Fig. 7) the dominant first shell Pb–F signal of the $Pb_{1-x}Sn_xF_2$ is broader than that for the β-PbF_2 standard (*13*), indicating an increased range of M–F distances from either thermal motion or static disorder. Since little change occurs in the Pb–L_3 EXAFS of $Pb_{0.7}Sn_{0.3}F_2$ between 77 and 300 K, static disorder is more important than thermal motion in determining the additional width of the Pb–F distance distribution.

The absence of a second coordination sphere of tin in the Sn–K EXAFS (Fig. 6) can be explained if the tin is displaced towards one of the faces of the F_8 cubes. This displacement can occur in six different directions. The statistical Pb/Sn disorder, combined with the disordered off-center lo-

TABLE V

SUMMARY OF PARAMETERS DERIVED FROM TWO COMPONENT ANALYSES OF FOURIER FILTERED FIRST-SHELL EXAFS

Species	Edge	Model	Parameter	Component 1	Component 2	Fit[a]
$PbSn_4F_{10}$ (300K)	Sn–K	SnO-300 K	R (Å)	2.05	2.19	4.7
			N	2.1	1.4	
			$\Delta\sigma^2(10^{-3}$ Å$^2)^b$	−7.2	−5.4	
			ΔE_0	2.9	2.9	
$Pb_{0.7}Sn_{0.3}F_2$ (300K)	Sn–K	SnO-300 K	R (Å)	2.03	2.15	4.1
			N	0.7	3.23	
			$\Delta\sigma^2(10^{-3}$ Å$^2)^b$	−9.7	−3.3	
			ΔE_0	−0.5	−0.5	
$Pb_{0.7}Sn_{0.3}F_2$ (77K)	Sn–K	SnO-300 K	R (Å)	2.11	2.16	5.1
			N	3.7	0.7	
			$\Delta\sigma^2(10^{-3}$ Å$^2)^b$	−1.2	0.1	
			ΔE_0	0.0	0.0	

[a] The sum of the squares of the differences between calculation and Fourier filtered experimental data, times 10^3.
[b] Difference in square of Debye–Waller term, relative to that of the model.

cation of each tin, results in a multitude of Sn–F, Sn–Sn and Sn–Pb distances beyond the first Sn–F sphere of coordination (Fig. 8), each with only a small contribution to the EXAFS signal. The presence of a large number of closely spaced distances precludes their detection.

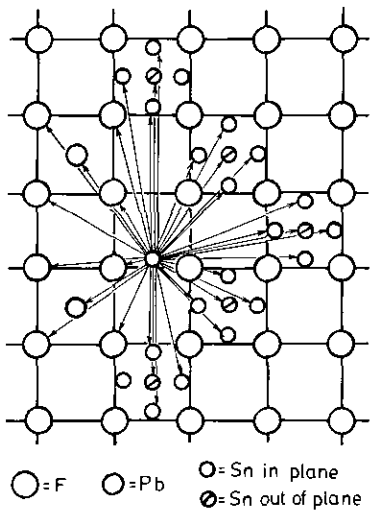

FIG. 8. Sketch of the local environment of tin in the disordered systems. Distances equal for symmetry reasons are not shown. The six possible locations of tin inside the F_8 cubes are taken into account.

In contrast, the Pb–L_3 EXAFS (Fig. 7) exhibits considerable signal at higher distances (2.8–4.8 Å). The shape of the Fourier filtered amplitude peaks at high k and is consistent with the second shell being a mixture of Pb and F backscatterers. The presence of a detectable Pb second shell signal around lead and the absence of any second shell signal around Sn is consistent with our understanding of the local structure of these species. The distances and coordination numbers for the higher ordered shells around Pb are listed in Table VI while a sketch of the Pb local environments is presented in Fig. 9. The Pb–Pb distances at 4.2 Å are observable because Pb is located at the center of the F_8 cubes and is not statistically disordered over several sites as is the Sn. Pb–Sn or Sn–Sn distances are not expected to be observable because the disorder over Sn positions in each F_8 cube gives a large number of such distances, each with a low probability. The second shell (shortest

TABLE VI

INTERATOMIC DISTANCES (<5 Å) FROM LEAD, CALCULATED FROM X-RAY DIFFRACTION

Atom 1–Atom 2	d (Å)	N		
		β-PbF_2	$PbSn_4F_{10}$	$Pb_{0.7}Sn_{0.3}F_2$
Pb–F	2.57	8	8	8
Pb–Sn	3.60	—	0.64	0.84
Pb–Pb	4.20	12	0.48	5.88
Pb–Sn	4.32	—	0.64	0.84
Pb–F	4.93	24	24	24
Pb–Sn	4.94	—	0.64	0.84
Pb–Sn	4.99	—	0.32	0.41

Note. The coordination number for the disordered systems ($PbSn_4F_{10}$ and $Pb_{0.7}Sn_{0.3}F_2$) was calculated taking into account (1) the probability of occupation of each cationic site by each cation; (2) the disorder of Sn over 6 positions in the occupied F_8 cubes; and (3) the multiplicity of each distance.

Pb–Pb distance) is fairly strong in β-PbF_2 (100% of the metal is Pb) and decreases as the lead content in the material is reduced (Fig. 7), as expected because of the low probability of two Pb atoms occupying adjacent cationic sites. Finally, second shell M–F distances (either Pb–F or Sn–F) are not expected to be observed because the fluorines of the second coordination sphere are likely to give local disordered shifts, thus resulting in a large number of distances, each of low probability.

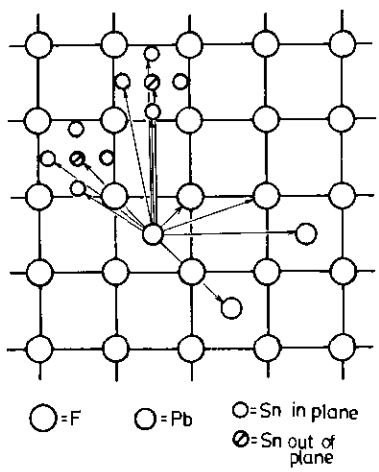

FIG. 9. Sketch of the local environment of lead in the disordered systems. Distances equal for symmetry reasons are not shown. The six possible locations of tin inside the F_8 cubes are taken into account.

As found in our earlier study of ordered $MSnF_4$ ionic conductors, the Pb–F average first shell distance (2.55(1) Å) is in good agreement with that expected from the sum of ionic radii (2.53 Å (29)), indicating that there is close-packed ionic bonding between Pb and F. In contrast the Sn–F average first shell distance (2.12(1) Å) determined from EXAFS is considerably shorter that the sum of ionic radii (2.26 Å (29)). This is consistent with previous evidence that Sn–F bonds in divalent tin fluorides have a significant amount of covalency (*30–33*). Partial overlap between the fluorine and tin valence orbitals brings the two atoms closer to each other than would be expected for two hard shell ions held near each other by electrostatic attraction only.

3.4. Structure and Fluoride Ion Mobility

The compounds investigated in this study present particularly challenging structural problems:

(i) The cubic solid solution shows no sign of order between tin and lead. Since the two metals cannot take the same type of coordination in this structure, considerable

local distortions must occur. They appear to be randomly distributed.

(ii) There is partial disorder between Pb and Sn in the tetragonal solid solution and β-$PbSnF_4$, along with a huge superstructure. However, only a few superstructure Bragg peaks are observed, and two different types of ordering occur, one along **c**, and another in the (**a**, **b**) plane.

(iii) Single crystals of these phases could not be obtained.

In the absence of precise structural data, it is hard to identify a unique mechanism for the increase in ionic conductivity as lead is substituted by tin. The disorder and local lattice distortion created by the substitution of some of the lead by tin most likely increase the amount of lattice defects and provide opportunities for fluoride ions to find temporary host sites with low barriers. As in α-$PbSnF_4$ and $BaSnF_4$, it is expected that more fluoride ion disorder occurs around tin than around lead, and this is certainly a key factor in the increase of conductivity with increasing tin content. However, the presence of tin also increases the disorder around lead. This interpretation is supported by the broad first-shell Sn–F and Pb–F EXAFS signals, which are associated with fluorine disorder around the metals. Furthermore, raising the temperature from 77 K to room temperature further broadens the peak in the FT magnitude without significant increase of the Debye–Waller factor. This shows that the fluorine disorder around tin is static and the amount of disorder increases with temperature.

In the absence of accurate three-dimensional structural data, it is difficult to locate the conduction pathway for the fluoride ions. However, two hypotheses can be proposed, based on our limited knowledge of their structure:

(i) Since the fluoride ions, on average, occupy the same sublattice as in β-PbF_2 and since the F_8 cubes not occupied by a metal are empty, the centers of these F_8 cubes (50% of the total F_8 cubes) are vacant and are therefore available for the formation of Frenkel defects, as in β-PbF_2,

(ii) Some of the fluoride ions coordinating tin can have a high mobility because of the large flexibility of the tin coordination. In addition to SnF_4E (E = lone pair) square pyramidal coordination (Fig. 5b), SnF_2E planar triangular and SnF_3E tetrahedral coordinations can also be obtained by a minor shift of tin in the fluorine cube, without shifting any fluorine atom. In addition, a local distortion of the SnF_4E square pyramid can give the well known SnF_4E triangular bipyramid, and a shift of a fluoride ion in a vacant F_8 cube can give a SnF_5E octahedron similar to that observed in α-$PbSnF_4$ and $BaSnF_4$. These alternative tin coordinations facilitate exchange of fluorine atoms between neighboring tin centers, which would result in a net fluoride ion displacement when an electric field was applied. Since this exchange mechanism would require tin ions on sites fairly close to one another, it becomes more likely as the probability of adjacent metal sites being occupied by tin increases; i.e., when the tin concentration in the sample is higher. In addition, exchange with the fluoride ions coordinating lead would also be expected to occur. These results are in agreement with the observation by ^{19}F NMR of the presence of two kinds of fluoride ions in cubic $Pb_{0.9}Sn_{0.1}F_2$, one mobile, the other rigid, with exchange occurring between the two kinds (*8*). The possibility of disordered multiple types of tin coordination is consistent with the broad first shell Sn–F signal and the absence of second shell signal in the Sn–*K* EXAFS.

Mössbauer spectroscopy shows that the tin lone pair is in a localized, stereoactive $5s^{2-x}5p^x$ hybrid orbital. Therefore the tin nonbonded electron pair cannot be transferred to a conduction band of the solid, and thus metal-like conductivity as in $CsSnBr_3$ (*27*) is not possible. This is consistent with transport number measurements, which give a rate of ionic (F^-) conduction larger than 0.99. The Mössbauer spectra are not inconsistent with the proposal of multiple tin coordination sites since the effect of bonding in tin(II) fluorides is often masked

by the much larger effect due to the hybridized lone pair. In addition, the low signal to background ratio in the Mössbauer spectra, which is due to the nonresonant absorption by the lead in these samples, precludes distinguishing between tin(II) sites with a similar hybridization and a stereoactive lone pair.

IV. Conclusion

We have used a combination of structural techniques to investigate the local site and overall crystal structure of $Pb_{1-x}Sn_xF_2$ (x = 0.3, 0.4, 0.5, and 0.8) fast ionic conductors. The investigation of their structure was more difficult than our earlier study of the ordered $MSnF_4$ species (*13*), because of the high degree of disorder. However, correlations between the X-ray diffraction, Mössbauer, and EXAFS results do provide useful insights into the structure of these materials, some of which are relevant to the ionic conduction mechanism. The most striking result is probably the exceptional ability of the β-PbF_2 fluorite structure to accept high substitution rates of cubic coordinated lead by tetracoordinated tin, without major structural reorganization. This generally occurs even without metal ordering, despite the large difference between the coordination of the two metals. The most surprising material is $PbSn_4F_{10}$, which has a highly unexpected regular fluorite type structure, even though 80% of the PbF_8 cubes, which are the building blocks and therefore the raison d'être of the fluorite type structure, have been replaced by SnF_4 square pyramids. It is as if 80% of the bricks from a wall were randomly replaced with jelly without affecting the overall structure of the wall. Of course, for this to be possible the structure had to accommodate a large amount of local distortions. However, these are randomly oriented and randomly distributed. All the materials investigated contain Pb(II) with a $6s^26p^0$ hybridization (unhybridized lone pair) and Sn(II) with a $5s^{2-x}5p^x$ hybridization (hybridized lone pair). The reasons for the difference of behavior between the two group 14 elements are (i) the larger size of lead which allows the lone pair to spread around the ion and therefore take the spherical symmetry of the 6*s* orbital, and (ii) the higher ionicity of lead.

The high fluoride ion mobility in these materials can be explained by the presence of a large number of empty F_8 cubes which enable the solid structure to tolerate a high density of Frenkel defects as in undoped β-PbF_2. Furthermore, the ability of tin(II) to take a variety of coordinations results in a high degree of fluorine disorder around tin and facilitates the exchange of fluoride ions between neighboring tin centers.

Acknowledgments

This research has been financed by NSERC (Canada), the Ontario Centre for Materials Research, and the Quebec Ministry of Higher Education (MESS) under the Programme d'Actions Structurantes. The authors thank the staff of the Cornell High Energy Synchrotron Source (CHESS) for their assistance. CHESS is supported by the U.S. National Science Foundation. GD acknowledges the support of an NSERC University Research Fellowship.

References

1. A. R. West, "Solid State Chemistry and its Applications," pp. 452–496, Wiley, New York (1984).
2. G. Denes, T. Birchall, M. Sayer, and M. F. Bell, *Solid State Ionics* **13,** 213 (1984).
3. G. Villeneuve and P. Hagenmuller, *Phys. Status Solidi B* **97,** 295 (1980).
4. G. Denes, J. Pannetier, and J. Lucas, *C. R. Acad. Sci. Ser. C* **280,** 831 (1975).
5. J. Pannetier, G. Denes, and J. Lucas, *Mater. Res. Bull.* **14,** 627 (1979).
6. T. Birchall, G. Denes, K. Ruebenbauer, and J. Pannetier, *Hyperfine Interact.* **29,** 1331 (1986).
7. M. Durand, J. Pannetier, and G. Denes, *J. Phys. (Paris)* **41,** 831 (1980).
8. C. Lucat, A. Rhandour, L. Cot, and J. M. Reau, *Solid State Commun.* **32,** 167 (1979).
9. G. Denes, *J. Solid State Chem.* **74,** 343 (1988).
10. C. R. A. Catlow, A. V. Chadwick, G. N. Greaves, and L. M. Moroney, *Nature* **312,** 601 (1984); C. R. A. Catlow, A. V. Chadwick, G. N. Greaves, and L. M. Moroney, *in* "Proc. EXAFS III" (K. O. Hodgson, B. Hedman, and J. K. Penner-Hahn, Eds.), p. 435, Springer-Verlag, Berlin/New York (1984).

11. P. O. BATTLE, C. R. A. CATLOW, A. V. CHADWICK, G. N. GREAVES, AND L. M. MORONEY, in "Proc. EXAFS IV," *J. Phys. Collog.* **47,** C8–669 (1986).
12. T. M. HAYES AND J. B. BOYCE, *J. Phys. C* **13** L731 (1980); T. M. Hayes and J. B. Boyce, *in* "EXAFS and Near Edge Structure" (A. Bianconi, L. Incoccia, and S. Stipcich, Eds.), Vol. 27, p. 182, Springer Series in Chemical Physics Springer-Verlag, Berlin/New York (1984); A. Yoshiasa, F. Kanamaru, S. Emura, and K. Koto, *Solid State Ionics* **27,** 267, 275 (1988); F. Rocca, G. Dalba, and P. Fornasini, *Mater. Chem. Phys.* **23,** 85 (1989).
13. G. DENES, Y. H. YU, T. TYLISZCZAK, AND A. P. HITCHCOCK, *J. Solid State Chem.* **91,** 1 (1991).
14. G. DENES, *J. Solid State Chem.* **77,** 54 (1988).
15. J. MONNIER, G. DENES, AND R. B. ANDERSON, *Can. J. Chem. Eng.* **62,** 419 (1984).
16. K. RUEBENBAUER AND T. BIRCHALL, *Hyperfine Interact.* **7,** 125 (1979).
17. A. P. HITCHCOCK, C. J. L. LOCK, AND B. LIPPERT, *Inorg. Chim. Acta* **124,** 101, (1986).
18. Y. H. YU, T. TYLISZCZAK, AND A. P. HITCHCOCK, *J. Phys. Chem. Solids* **51,** 445 (1990).
19. D. E. SAYERS AND B. A. BUNKER, Data Analysis, *in* "Chemical Analysis 92" (D. C. Koningsberg and R. Prins, Eds.), p. 211, Wiley, New York (1988).
20. P. A. LEE, P. H. CITRIN, P. EISENBERGER, AND B. M. KINCAID, *Rev. Mod. Phys.* **53,** 769 (1981).
21. J. MUSTRE DE LEON, Y. YACOBY, E. A. STERN, AND J. J. REHR, *Phys. Rev. B* **42,** 20,843 (1990); J. J. Rehr, J. Mustre de Leon, S. I. Zabinsky, and R. C. Albers, *J. Am. Chem. Soc.* **113,** 5135 (1991).
22. J. Y. LE MAROUILLE, THÈSE DE 3ième Cycle, Université de Rennes I, Rennes (1972).
23. T. BIRCHALL, G. DENES, K. RUEBENBAUER, AND J. PANNETIER, *J. Chem. Soc. Dalton Trans.,* 1831 (1981).
24. R. J. GILLESPIE AND R. S. NYHOLM, *Q. Rev. Chem. Soc.* **11,** 339 (1957).
25. J. GALY, G. MEUNIER, S. ANDERSSON, AND A. ASTRÖM, *J. Solid State Chem.* **13,** 142 (1975).
26. I. D. BROWN, *J. Solid State Chem.* **11,** 214 (1974).
27. J. D. DONALDSON AND J. SILVER, *J. Chem. Soc. A,* 666 (1973).
28. J. PANNETIER AND G. DENES, *Acta Crystallogr. Sect. B* **36,** 2763 (1980).
29. R. C. WEAST, ED., "CRC Handbook of Chemistry and Physics," 61st ed., p. F-216, CRC Press, Boca Raton, FL (1980–1981).
30. G. DENES, *Mater. Res. Bull.* **15,** 807 (1980).
31. G. DENES, J. PANNETIER, J. LUCAS, AND J. Y. LE MAROUILLE, *J. Solid State Chem.* **30,** 335 (1979).
32. G. DENES, J. PANNETIER, AND J. LUCAS, *Solid State Chem.* **33,** 1 (1980).
33. G. DENES, *J. Solid State Chem.* **36,** 20 (1981).